1989

Barotropic Shelf Circulation Forced by an Isolated Oceanic Disturbance.

Xinyu He
Louisiana State University and Agricultural & Mechanical College

Order Number 9017264

Barotropic shelf circulation forced by an isolated oceanic disturbance

He, Xinyu, Ph.D.

The Louisiana State University and Agricultural and Mechanical Col., 1989

U·M·I
300 N. Zeeb Rd.
Ann Arbor, MI 48106

BAROTROPIC SHELF CIRCULATION FORCED BY AN ISOLATED OCEANIC DISTURBANCE

A Dissertation

Submitted to the Graduate Faculty of the
Louisiana State University and
Agricultural and Mechanical College
in partial fulfillment of the
requirements for the degree of
Doctor of Philosophy

in

The Department of Marine Sciences

by
Xinyu He
B.S., Jilin University, China, 1982
M.S., Ocean University of Qingdao, China, 1985
August 1989

ACKNOWLEDGMENTS

I should like to thank my committee members for their helpful assistance. I should especially like to thank my major professor, Dr. Wiseman, for his valued discussions, suggestions and support.

This dissertation is dedicated to my beloved mother.

CONTENTS

Acknowledgments iv

Abstract v

Chapter I: Introduction 1

Chapter II: Formulation 5

Governing equations 5
Boundary conditions 10
General solution 12

Chapter III: Solution for the Linear Shelf Profile . . . 18

Straight shelf topography h=h(x) 20
Curved shelf topography h=h(x,y) 30

Chapter IV: Discussion 40

Chapter V: Conclusions 52

Appendix A: An Integral Theorem 54

References 57

Vita 61

ABSTRACT

A 'slowly varying' and 'isolated' oceanic disturbance may locally drive the shelf circulation. This situation is analytically studied using a linear, steady-state, barotropic model. The solution has a dipolar structure over the shelf. This is consistent with an integral theorem of zero net relative angular momentum on the f-plane with a sloping topography, derived herein. It is found that the forced circulation patterns are controlled by the alongshore scale of the disturbance, magnitude of bottom stress, and geometry of the shelf. In particular, by generating significant relative vorticity due to the ageostrophic motion, the friction strongly influences the center position, the strength, and the size of the forced shelf motion. When large alongshore topographic variations are present, the combined effect of the friction and shelf curvature results in an asymmetry of the pressure field, with an intensified motion inshore.

Chapter I

INTRODUCTION

In recent years there has been considerable interest in ocean-driven shelf circulation. The oceanic forcing may often take the form of an isolated mesoscale feature. Although eddies and meanders of the deep-ocean flow are regularly observed over the continental shelf, their dynamics and impacts on the shelf circulation are not fully understood.

There is worldwide observational evidence of oceanic eddies/meanders approaching the coast. A distinct example frequently reported is the existence of Gulf Stream rings interacting with the shelf. For instance, a Gulf Stream warm-core ring encountered the northeast coast of the U.S. in 1983. A cyclonic eddy and shelf/slope water exchange were associated with the ring (Churchill et al., 1986). Similarly, strong eddy-related currents over the shelf and slope were observed in the East Australian Current region during the Australian Coastal Experiment (Huyer et al, 1988). Frontal eddies are also common phenomena. These eddies have the potential for locally enhancing water exchange between the shelf and the slope (Garvine et

al,1988). At times, a meander of the deep-ocean flow may intrude onto the shelf and have significant influence on coastal and shelf water (e.g., Huh et al, 1981). These observations have been challenging ongoing studies on the dynamics of shelf/ocean interaction.

Previous analytical studies of the related problems are few. Csanady (1978) showed, using a linear, steady, barotropic model, that a large-scale alongshore pressure gradient imposed by the open ocean at the shelf break could drive shelf currents. In this model, the cross-shelf bottom stress and alongshore topographic variation were neglected. Real world scenarios are readily formulated where neither of these assumptions may be physically plausible. Using a depth-averaged barotropic model, Middleton (1987) quantitatively investigated the steady coastal response to alongshore oceanic pressure gradients. For linear and parabolic depth profiles, he showed that on narrow continental margins, oceanic pressure fields are easily transmitted to the coast. There are also several numerical studies of various aspects of the ocean-driven shelf and slope circulation. Smith (1986) examined the interaction of Loop Current eddies with the continental slope region in the Gulf of Mexico by using a two-layer primitive-equation numerical model, and he indicated that eddy asymmetry can be induced by a lateral boundary. Using a linear, steady, baroclinic numerical model, Kelly and Chapman (1988) concluded that a deep-ocean

eddy can create an alongshore jet trapped over the upper slope, but that the eddy does not significantly affect the shelf circulation. However, two important questions remain unanswered: 1) how does an isolated oceanic disturbance which penetrates to the shelf break influence the shelf circulation? 2) what would be the effect of a curved shelf topography? It presently appears that there are no analytical studies specifically exploring these problems.

Although the eddy field is often baroclinic, to the first approximation, the velocity field over the shelf may be considered to be barotropic, as supported by observations and theoretical studies, e.g., Louis and Smith, 1982; Kelly and Chapman, 1988. Hence, the properties of shelf circulation forced by an isolated oceanic disturbance are studied here using a simple, barotropic, analytic theory. This work closely follows that of Csanady (1978). The main difference between this work and Csanady's work lies in the considerations of the isolated oceanic forcing and large longshore topographic variations. Several assumptions will be made to simplify the problem. These assumptions are based on the following concepts: (1) the disturbance is 'slowly varying', i.e., the evolution time scale of the disturbance is much longer than the inertial and spin-up periods, and, (2) the disturbance is 'isolated', i.e., the disturbance is of limited longshore extent. These fundamental concepts appear reasonable based on direct observations of ocean eddies.

This work consists of five chapters and an appendix. The formulation of the problem is presented in chapter 2. Solutions for a linear shelf profile, with straight and curved shelf topographies, are given in chapter 3. The results are discussed in chapter 4, and conclusions are drawn in chapter 5. An integral theorem of zero net relative angular momentum for the isolated system on the f-plane is proved in the appendix.

Chapter II

FORMULATION

Circulation over the continental shelf may be partially driven by oceanic forcing. Furthermore, the interaction of an isolated oceanic disturbance with varying shelf topography may produce a variety of resultant circulation patterns. The model presented here represents an attempt to study the pattern of steady shelf circulation forced by such a disturbance. In the linear formulation, oceanic forcing and local wind stress can be considered to be independent. Therefore, wind stress is taken to be zero in the present study.

2.1 Governing equations

Consider a barotropic model of an idealized continental shelf with sloping bottom topography. Choose a right-handed Cartesian coordinate system such that the positive x-axis points seaward from the coast, the y-axis is perpendicular to the left of the x-axis, and the positive z-axis is vertically up (Fig. 2.1). In the region considered, the depth, h, of the ocean is a function of both offshore and longshore distance, i.e., $h = h(x,y)$. It is desired to study ocean-forced, frictionally-dominated mean flow over such a shelf.

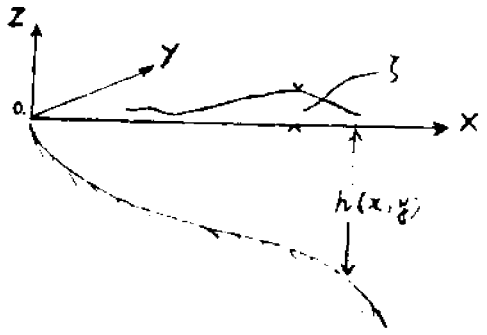

Figure 2.1: The geometry used in the model.

The steady, linearized, viscid, vertically (z)-integrated equations of motion have the form

$$-fV = -g\frac{\partial \zeta}{\partial x} - \frac{T_{bx}}{\rho h}, \qquad (2.1)$$

$$fU = -g\frac{\partial \zeta}{\partial y} - \frac{T_{by}}{\rho h}, \qquad (2.2)$$

$$\frac{\partial (hU)}{\partial x} + \frac{\partial (hV)}{\partial y} = 0, \qquad (2.3)$$

where U and V are the depth-averaged components of velocity in the x and y directions, respectively, ζ is the vertical displacement of the sea surface above the equilibrium level, T_{bx} and T_{by} are the x and y components of bottom stress, g is the acceleration due to gravity, ρ is the den-

sity of sea water, and f is the Coriolis parameter, assumed to be constant. By taking the curl of (2.1) and (2.2), and using (2.3), the vorticity balance of the flow is

$$-(\nabla\times \tau_b/\rho) + g\nabla\zeta\times\nabla h = 0. \qquad (2.4)$$

Because alongshore variations in topography are allowed ($h_y \neq 0$), $g\,\zeta_x h_y$ appears in (2.4) as a vorticity source term ignored in many previous models of shelf circulation, e.g., Csanady(1978). Relative vorticity is generated by stretching or squashing of fluid columns when they move in the y-direction. This, together with the more common vortex change due to stretching associated with motion in the x-direction, must balance the curl of the bottom stress to maintain a steady vorticity distribution.

Bottom friction is assumed to be proportional to the depth-averaged velocity (Csanady, 1978),

$$\frac{\tau_{bx}}{\rho} = rU, \qquad \frac{\tau_{by}}{\rho} = rV, \qquad (2.5)$$

where r is a bottom friction coefficient with dimensions of velocity. Substitution of (2.5) into (2.1)and (2.2) produces

$$U(1+r^2/f^2h^2) = -\frac{g}{f}\frac{\partial\zeta}{\partial y} - \frac{rg}{f^2h}\frac{\partial\zeta}{\partial x},$$

$$V(1+r^2/f^2h^2) = \frac{g}{f}\frac{\partial\zeta}{\partial x} - \frac{rg}{f^2h}\frac{\partial\zeta}{\partial y}.$$

If the terms associated with $(r/fh)^2$ in the above equations are neglected, and U, V are eliminated from (2.3), then there are a set of three linear equations for ζ, U and V,

$$\zeta_{xx} + \zeta_{yy} + (\zeta_y h_x - \zeta_x h_y)\, f/r = 0, \qquad (2.6)$$

$$U = -\frac{g}{f}\frac{\partial \zeta}{\partial y} - \frac{rg}{f^2 h}\frac{\partial \zeta}{\partial x}, \qquad (2.7)$$

$$V = \frac{g}{f}\frac{\partial \zeta}{\partial x} - \frac{rg}{f^2 h}\frac{\partial \zeta}{\partial y}. \qquad (2.8)$$

It has been assumed in deriving (2.6), (2.7) and (2.8) that

$$(r/fh)^2 \ll 1, \qquad (2.9)$$

which is satisfied if h is much larger than the ratio, r/f. The inequality (2.9) usually holds for the regions under consideration. The neglected terms in the momentum equations are small, second-order ones associated with the viscous friction. The condition (2.9) implies that motion very near the coast (h = 0) is excluded in the present model. The inshore boundary of the model domain is defined by the ratio, r/f. The effect of this condition will be discussed in the later chapters.

In the subsequent analysis, the simplifying assumption is made that the term ζ_{yy} in (2.6) can be neglected. A condition for the neglect of this term can be obtained by scaling the vorticity equation (2.6). Introducing the following nondimensional variables

$$x' = x/L_x, \quad y' = y/L_y, \text{ and } \quad h' = h/h_0$$

into (2.6) and dropping the primes results in a nondimensional equation ,

$$\zeta_{xx} + \delta^2 \zeta_{yy} + C(\zeta_y h_x - \zeta_x h_y) = 0,$$

where δ^2 and C are dimensionless parameters,

$$\delta^2 = (L_x / L_y)^2, \text{ and}$$

$$C = f h_0 / r(L_x / L_y),$$

L_x and L_y are cross- and along-isobath length scales,respectively, and h_0 is the depth scale of the shelf. For typical shelf circulation scales where L_x = 100km, L_y = 1000km, f = 0.0001/s, r = 0.0005m/s, and h_0 = 100m, it is estimated that

$$\delta^2 \ll 1, \text{ and}$$

$$C \geq 1.$$

However, it should be pointed out that, because the oceanic forcing and the shelf topography may have different length scales, designated by L_{yo} and L_{yt}, respectively, the above condition for δ^2 must satisfy

$$\text{maxim}[(L_x / L_{yo})^2, (L_x / L_{yt})^2] \ll 1. \qquad (2.10)$$

For example, if an oceanic disturbance has a length scale of 400km, (2.10) may still be a good approximation provided L_x $\leq$ 100km. Therefore the second term in (2.6) is neglected under the condition (2.10), yielding

$$\zeta_{xx} + C (\zeta_y h_x - \zeta_x h_y) = 0. \qquad (2.11)$$

which is to be solved to provide a picture of the pressure field. It is clear from (2.11) that the vortex stretching due to alongshore motion can be as important as that due to cross-shelf motion in generating the pressure field over the shelf, if significant longshore topographic variations are present.

2.2 Boundary conditions

The next problem is to solve (2.11) for given boundary conditions on ζ. Hereafter boundary conditions are also nondimensionlized using the same scaling as in the above discussion. Fig.1 shows the geometry of the model. The inshore boundary must occur at water depths consistent with (2.9). For simplicity, a constant depth contour, consistent with (2.9), is selected. The corresponding x-coordinate will be taken, without losing generality, as $x = L_1(y)$. In particular, for a straight coastline, $L_1(y) = 0$. At the inshore boundary, $x = L_1(y)$, a simple boundary condition is imposed

$$\zeta = 0. \qquad (2.12)$$

The boundary condition (2.12) is not necessary, in contrast to a boundary condition frequently used by previous investigators, to require the constraint of zero-normal flow near the coast (Mitchum and Clarke, 1986). Since there is no wind stress for this problem, as discussed at the begining

of this section, the surface Ekman layer does not exist. Thus there is no interaction of the surface and bottom Ekman layers. Therefore, it would be difficult to define the location at which the normal mass transport becomes zero. It might be so near the coast and it should be so at the coast. It is argued here that (2.12) arises because the isolated ocean-forced pressure field tends to decay approaching the coast due to topographic constraints and frictional dissipation. This contention is supported by observations and theoretical studies. For example, Huyer et al. (1988) found that coastal sea-levels were not strongly affected by the East Australian Current eddies and meanders. Kelly and Chapman (1988), using their numerical model, showed that the penetration of ocean-forced energy drops dramatically as the coast is approached. Hence (2.12) is chosen in this study because of its mathematical simplicity and supporting observations. It is assumed to be a reasonable inshore-boundary condition for isolated ocean-forced shelf motion.

At the offshore boundary, $x = L_2(y)$, the oceanic pressure forcing is specified as

$$\zeta = f(y). \qquad (2.13)$$

It is required that $f(y)$ have the character of an isolated disturbance. It is further assumed that $h(L_2(y), y)$ is constant.

At the open boundary, y = 0, because of the assumption of isolated forcing, it is assumed that

$$\zeta = 0. \qquad (2.14)$$

Equation (2.11) is a parabolic equation for ζ, thus no downstream boundary condition for y is needed.

2.3 General solution

The form of equation (2.11) suggests the use of new non-dimensional coordinates (ξ,η), where the variables ξ and η are defined by

$$\left.\begin{aligned} \xi &= f(x,y) \\ \eta &= y \end{aligned}\right\}. \qquad (2.15)$$

The transformation (2.15) will be required to have a non-vanishing Jacobian ,

$$\frac{\partial(\xi,\eta)}{\partial(x,y)} \neq 0.$$

The f(x,y) in (2.15) can be chosen to describe different variations in shelf topography. The problem for alongshore topographic variations is formulated by assuming that the water depth over the shelf is given, in dimensionless form, by

$$h = h(\xi). \qquad 0 \leq \xi \leq 1 \qquad (2.16)$$

The lines of constant ξ are constant depth contours on the continental shelf. The inshore edge of the domain is set at

$\xi = 0$ and the shelf break is set at $\xi = 1$. It is assumed that the contours of constant depth are uniquely defined and continuous. A variety of shelf profiles may be selected such as the linear shelf profile

$$h(\xi) = h_1 + s\xi,$$

or the exponential shelf profile

$$h(\xi) = h_1 \exp(k\xi).$$

By choosing the parameters h_1, s, and k appropriately, reasonable fits to actual shelf topographies may be made.

By changing coordinates from (x,y) to (ξ,η), equation (2.11) with its more general boundary conditions become

$$\frac{\partial^2 \zeta}{a(\xi)\partial \xi^2} + \frac{\partial \zeta}{b(\eta)\partial \eta} = f_0(\xi,\eta), \qquad (2.17)$$

$$\left.\begin{array}{l} G\left(\zeta, \dfrac{\partial \zeta}{\partial \xi}\right) = f_1(\eta) \quad \text{at } \xi = 0 \\ \zeta = f_2(\eta) \quad \text{at } \xi = 1 \\ \zeta = f_3(\xi) \quad \text{at } \eta = 0 \end{array}\right\}, \qquad (2.18)$$

where $a(\xi) = \partial h/\partial \xi$, $b(\eta) = C\,\xi_x$, $G(\zeta, \partial\zeta/\partial\xi)$ denotes the first, or the second, or the third kind boundary condition of the parobolic equation, $f_0(\xi,\eta)$ is an interal forcing function, $f_1(\eta)$, $f_2(\eta)$, and $f_3(\xi)$ are functions determined by the boundary conditions. In deriving (2.17), it is assumed that

$$\xi_{xx} = 0. \qquad (2.19)$$

This condition severely restricts how the function $f(x,y)$ is chosen. The dominant physics, however, are retained even for simple bathymetric profiles such as a linear shelf profile. For example, Middleton (1987) showed that for the linear and parabolic depth profiles the patterns of the flow due to an oceanic pressure field were similar. Thus, the problem for ζ over the shelf is defined by the equations (2.17) and (2.18), which will be solved by an eigenfunction expansion. Note that under the transformation (2.15), the system (ξ,η) is transformed from (x,y) without assuming small-amplitude longshore variations in topography, as was done by Csanady (1978) for the arrested topographic wave, and by Allen (1976) for barotropic continental shelf waves. This transformation would be applicable to both large and small alongshore changes.

Let

$$\zeta = \Phi(\xi,\eta) + \phi(\xi,\eta),$$

where ϕ satisfies (2.17) and the boundary condition on ξ

$$\left.\begin{aligned} G(\phi, \partial\phi/\partial\xi) &= f_1(\eta) \quad \text{at } \xi = 0 \\ \phi &= f_2(\eta) \quad \text{at } \xi = 1 \end{aligned}\right\} .$$

Then Φ satisfies

$$\left.\begin{aligned} \frac{\partial^2\Phi}{a(\xi)\partial\xi^2} + \frac{\partial\Phi}{b(\eta)\partial\eta} &= F(\xi,\eta) \\ G\left(\Phi, \frac{\partial\Phi}{\partial\xi}\right) &= 0 \quad \text{at } \xi = 0 \\ \Phi &= 0 \quad \text{at } \xi = 1 \\ \Phi &= F_3(\xi) \quad \text{at } \eta = 0 \end{aligned}\right\} , \qquad (2.20)$$

where

$$F(\xi,\eta) \equiv f_0(\xi,\eta) - (\partial^2\phi/\partial\xi^2)/a(\xi) - (\partial\phi/\partial\eta)/b(\eta),$$

$$F_3(\xi) \equiv f_3(\xi) - \phi(\xi,0).$$

Suppose $F(\xi,\eta)$ can be decomposed such that

$$F(\xi,\eta) = \sum_{n=0}^{\infty} F_n(\eta)X_n(\xi), \qquad (2.21)$$

where $X_n(\xi)$ are the eigenvectors of the Sturm-Liouville system found when solving the associated homogeneous problem to (2.20) by separation of variables. Assuming

$$\Phi(\xi,\eta) = X(\xi)Y(\eta),$$

the Sturm-Liouville problem is

$$\left.\begin{aligned} &X'' + \lambda^2 a(\xi)X = 0 \\ &w(X, X') = 0 \qquad \text{at } \xi = 0 \\ &X = 0 \qquad \text{at } \xi = 1 \end{aligned}\right\}, \qquad (2.22)$$

where λ is the eigenvalue, $a(\xi)$ is the weighting function, and $w(X, X') = pX + qX'$, with $p^2 + q^2 \geq 0$. This is the general set of boundary conditions for the Sturm-Liouville problem. In some cases, an exact solution can be found for (2.22). In other cases, an approximate solution may be obtained, e.g., an asymptotic expression for $X(\xi)$ (Morse and Feshbach, 1953).

Once the eigenvectors of (2.22) are found, replacing $F(\xi,\eta)$ by (2.21) in (2.20), the equation for $Y(\eta)$ takes the form

$$\left.\begin{aligned} Y' - \lambda^2 b(\eta) Y &= F_n^*(\eta) \\ \sum_{n=0}^{\infty} Y_n(0) X_n(\xi) &= F_3(\xi) \end{aligned}\right\} , \quad (2.23)$$

where

$$F_n^*(\eta) = F_n(\eta)\ b(\eta),$$

$$Y_n(0) = \int_0^1 F_3(\xi) a(\xi)\ X_n(\xi)\ d\xi \ /$$

$$\int_0^1 a(\xi)\ X^2{}_n(\xi)\ d\xi \equiv a_n \ .$$

The solution of (2.23), using an integrating factor, is

$$Y_n(\eta) = a_n\ e_+ + e_+ \int_0^{\eta} e_-\ F_n^*(\eta')\ d\eta', \qquad (2.24)$$

where

$$e_+ = \mathrm{Exp}\left(\int_0^{\eta} \lambda^2 b(\eta')\ d\eta'\right),$$

$$e_- = \mathrm{Exp}\left(\int_0^{\eta} -\lambda^2 b(\eta')\ d\eta'\right).$$

Finally, the total solution for ζ is obtained

$$\zeta = \Psi(\xi,\eta) + \phi(\xi,\eta)$$

$$= \sum_{n=0}^{\infty} X_n(\xi) Y_n(\eta) + \phi(\xi,\eta). \qquad (2.25)$$

It is interesting to see that since factors involving topographic variation, $a(\xi)$ and $b(\eta)$, have entered the equation (2.17), they will influence the solution (2.25) for the

pressure field, ζ. Any change of the pressure gradient, however, will alter the structure of the flow field over the shelf. Hence, the interaction between the forced flow field and shelf topographies should be extensively explored. Also, it should be noted that other boundary conditions besides (2.18) may be imposed. In principle, this does not bring more mathematical difficulty to the problem. The eigenfunction expansion method can be generally applied.

Chapter III

SOLUTION FOR THE LINEAR SHELF PROFILE

In this section the formalism derived in the previous chapter is applied to determine the shelf response to an isolated oceanic disturbance interacting with a varying shelf topography. A linear shelf profile is assumed here, offering special analytical simplicity for theoretical study, yet maintaining the important process of vortex stretching. The offshore boundary is assumed to be straight, i.e., its dimensionless form is $x = 1$. The oceanic forcing is assumed to be a Gaussian pressure field imposed at the shelf break, i.e., in (2.13) the dimensionless pressure function is

$$f(y) = \exp(-(y+A)^2 B), \qquad (3.1)$$

where $(1,-A)$ is the position of the disturbance center and B is a nondimensional parameter such that

$$B = (L_y/\sigma)^2, \qquad (3.2)$$

where σ is the dimensional alongshore scale of the forcing.

Before applying the model to a specific case, it is necessary to consider the parameter space in which the model is valid. There are two nondimensional parameters in the

study: the external parameter B in (3.2), characterizing the forcing; the internal parameter C in (2.11),

$$C = (L_x/L_y)\, fh_0/r, \text{ or } (L_x/\sigma) fh_0/r,$$

affecting the distribution of the shelf pressure field. Typical parameter values for realistic conditions over the shelf are considered in the following study. The oceanic disturbances have spatial scales from a few tens of kilometers which is the scale of frontal eddies (Garvine et al, 1988), to a few hundred kilometers, such as Gulf Stream rings (Churchill, et al, 1986) or Gulf Stream meanders (Brooks and Bane, 1983). The frictional coefficient, r, has values observed in the range of $0.0001m/s < r < 0.001m/s$, eg., r is about 0.0004m/s on the west Florida shelf (Kroll and Niiler, 1976), and 0.001m/s on the eastern U.S. shelf (Csanady, 1978). The geometric scales of the shelf vary widely: $50m < h_0 < 200m$, $40km < L_x < 200km$ and $300km < L_y < 1000km$. For instance, the west coast of U.S. has generally narrow and steep shelves with $L_x = 40km$ and $h_0 = 200m$; the east coast has broad and flat shelves with $L_x = 100km$ and $h_0 = 100m$ (Kennett, 1982). The Coriolis parameter lies in the range $0 < f < 2\times7.3\times0.00001/s$. The above combinations of parameters then give the values for the two parameters B and C. The solutions we seek are restricted to the parameter range for which the two conditions, (2.9) and (2.10), under which the equation (2.11) was derived, must be met. Fig. 3.1 shows the parameter space in this study.

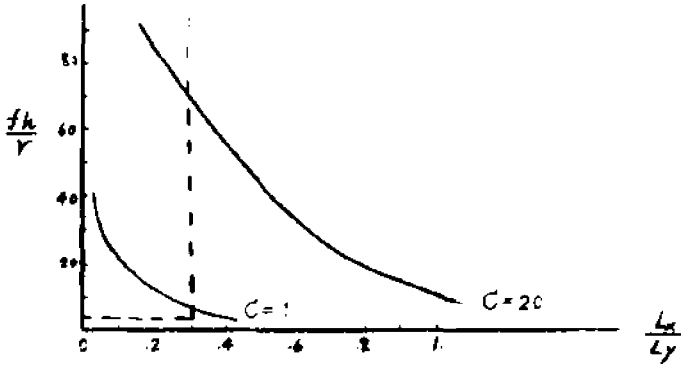

Figure 3.1: The parameter space. The dashed lines define the valid range of the model.

3.1 Straight shelf topography h=h(x)

Consider a simple shelf topography such that depth increases with increasing x only. In spite of this ideal simplification, illuminating insights into the important physics may still be obtained. For this topography, the longshore length scale, L_y, is assumed to be a longshore wavelength appropriate to barotropic topographic Rossby waves, because eddies or meanders encountering the continental margin may generate wavelike motions. In such cases, a certain wavelength could predominate over the shelf, as suggested by observations and theoretical studies (Kroll and Niiler,1976; Garrett, 1979; Louis and Smith, 1982). Thus, it is assumed in the following study that L_y is approximately of the same order as the longshore scale of the disturbance, i.e., $L_y/\sigma \sim 1$. The nondimensional solution for sea level, ζ, is, as discussed in chapter 2,

$$\zeta = \sum_{n=1}^{\infty} X_n(x)Y_n(y) + x\exp(-(y+A)^2B), \quad (3.3)$$

where

$$X_n(x) = \sin(n\pi x), \quad n = 1,2,3,\ldots,$$

$$Y_n(y) = a_n e_+ + e_+\int_0^y e_- F_n^*(y')\,dy'$$

in which a_n, e_+ and e_- are analytically calculated. The variables, U and V, are obtained from (2.7) and (2.8).

Generally, the solution to the imposed oceanic disturbance is an anticyclonic (cyclonic) motion near the shelf break and a cyclonic (anticyclonic) motion inshore, i.e., a modon-like solution. This steady pattern is now discussed in terms of vorticity. A detailed discussion of the generation mechanism for this circulation is beyond the scope of the present study. The vorticity equation (2.4) expresses a balance between the torque developed by the pressure gradient acting on a sloping bottom and the curl of the frictional stress. This is relatively uninformative, but is more readily understandable when the total velocity field is separated into two parts, $U = U_g + U_e$, $V = V_g + V_e$, so that the momentum equations (2.1) and (2.2) become

$$-fV_g = -gh\,\zeta_x, \quad -fV_e = -T_{bx}/\rho;$$

$$fU_g = -gh\,\zeta_y, \quad fU_e = -T_{by}/\rho.$$

where the subscripts, g, e, denote the geostrophic and Ekman velocity components, respectively. The curl of these equations yields

$f\nabla\cdot M_g = g\nabla\zeta\times\nabla h$, $f\nabla\cdot M_e = -\nabla\times \tau_b/\rho$,

where M_g and M_e are geostrophic and bottom Ekman layer mass transports. Since $\nabla\cdot M_e = -w_e$, where w_e is the vertical velocity at the top of the bottom Ekman layer, the vorticity equation (2.4) may be rewritten in the form

$$(\nabla\zeta\times\nabla h)g/f - w_e = 0. \qquad (3.4)$$

The above analysis shows that this frictionally-induced vertical velocity associated with the convergence or divergence of the Ekman transport will balance the vorticity production by vortex-tube stretching. In the present study, this vertical velocity is not explicitly resolved in the vertically-integrated momentum equations, and its action is reflected parametrically through the curl of the frictional stress. The stress is parameterized using (2.5), thus, its curl is related to the Laplacian of the sea surface displacement in equation (2.6). Hence, the sea surface must distort in such a way as to produce pressure gradients that maintain the steady vorticity distribution. It may also be helpful to understand the solution by considering the derived integral constraint for this isolated system (see appendix).

To examine the dynamic effects of various parameters of the problem on the steady motion, several numerical experiments are carried out (see Table 3.1). First, the effect of varying the friction coefficient is examined. Given f = 0.0001/s, L_x = 100km, and h_o= 100m, the results for two

values of the friction coefficient, r = 0.0001m/s and r = 0.0005m/s, are shown in Fig. 3.2. The dimensional x-unit is 100km. For a fixed f, the ratio r/f varies as r changes. Thus, the inshore model boundary must occur at different water depths consistent with the condition (2.9), $(r/fh)^2 \ll 1$. For r = 0.0001m/s, the inshore boundary was placed at the water depth h_1 = 5m, which is sufficient to satisfy (2.9), i.e., $(r/fh_1)^2 = (1/5)^2 \ll 1$. Thus, the boundary condition (2.12) is applied at x_1 = 5km from the coast. Now the parameter C is rescaled. $C = (fh'/r)\, L'_x/L_y$, where $h' = h_0 - h_1$, $L'_x = L_x - x_1$, so that C = 15. Similarly, for r = 0.0005m/s, the inshore boundary occurs at the water depth h_1 = 25m, and C = 2. The solutions are quite different. For small r (Fig. 3.2a), the disturbance intrudes further shoreward, and a weak, broad cyclonic motion occurs inshore in response to the forcing. For large r (Fig. 3.2b), the disturbance intrudes less far shoreward, and a strong, narrow cyclonic motion occurs inshore. These patterns can be explained in terms of our understanding of the vorticity balance (3.4). Larger friction will cause greater mass flux in the thicker bottom boundary layer for given pressure gradients. This thicker Ekman layer is able to accept or provide a greater vertical mass flux, thus balancing stronger vortex stretching outside the boundary layer due to higher velocities and stronger pressure gradients. However, stronger friction implicitly requires a greater rate per

unit area at which work is done by the pressure force in the Ekman layer, i.e., stronger friction will dissipate more energy in the Ekman layer. The energy source is supplied by the imposed disturbance at the offshore boundary. Since a given forcing is isolated in space, total energy input by the forcing per unit time is finite; therefore, for this fixed rate of

Table 3.1: Parameter values used in the experiments.

Varying Parameters	Constant Parameters	Nondimensional Parameters
a1 $r = 1*10^{-4}\ ms^{-1}$ a2 $r = 5*10^{-4}\ ms^{-1}$	$f = 10^{-4}\ s^{-1}$ $L_x = 100$ km $L_y = 600$ km $h_0 = 100$ m	C = 15.0 B = 1.0 C = 2.0 B = 1.0
b1 $L_x = 100$ km b2 $L_x = 50$ km	$f = 10^{-4}\ s^{-1}$ $r = 10^{-4}\ ms^{-1}$ $L_y = 600$ km $h_0 = 100$ m	C = 15.0 B = 1.0 C = 7.0 B = 1.0
c1 $\sigma = 300$ km c2 $\sigma = 600$ km	$f = 10^{-4}\ s^{-1}$ $r = 5*10^{-4}\ ms^{-1}$ $L_x = 100$ km $h_0 = 100$ m	C = 4.0 B = 4.0 C = 2.0 B = 1.0

energy supply, motion with stronger friction will occur within a 'narrower' area than will motion with weaker friction. Friction also influences the center position, the strength, and the size of the inshore eddy. Hereafter the strength is measured by the central sea surface depression of the inshore eddy. The central position and depression of

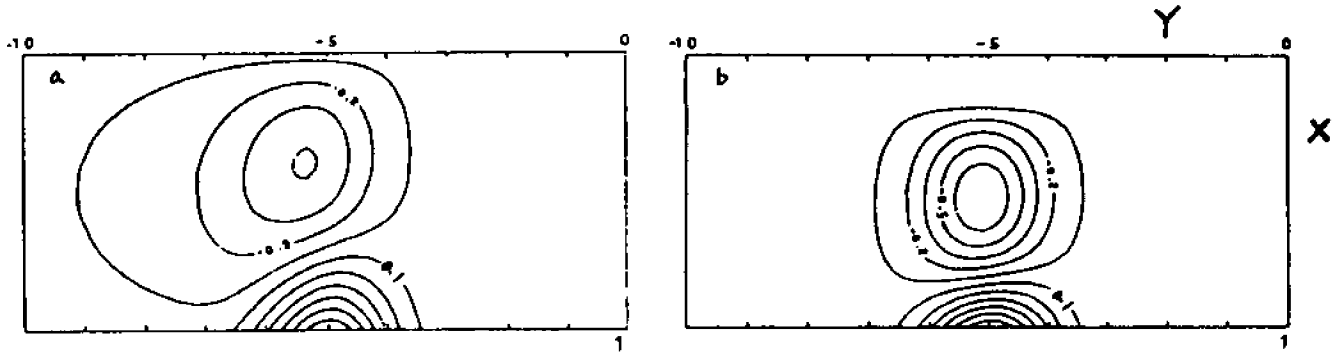

Figure 3.2: The dimensionless pressure field for a) r=0.0001m/s, and b) r=0.0005m/s. The forcing is imposed at x = 1.

the inshore eddy were determined numerically to produce Fig. 3.3. As r increases, the center of the eddy moves toward the shelf break and the central depression increases. The motion is more spatially confined over the shelf,

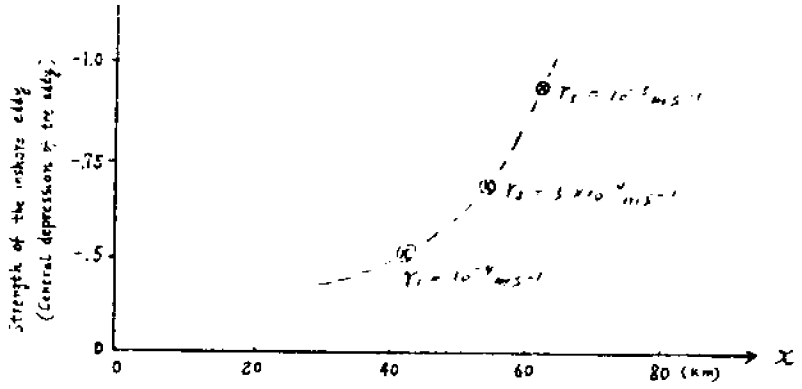

Figure 3.3: The effect of bottom friction on the center and the strength of the inshore circulation.

as discussed above. Note that in Fig.3.3 , the movement of the inshore eddy center toward the shelf break may also be due to seaward migration of the inshore boundary in accordance with the condition (2.9). However the displacement of the eddy center is not proportional to the displacement of the inshore boundary, thus the friction coefficient is considered as a significant dynamic factor. It is obvious from Fig. 3.2 that as r decreases, the edge of the inshore eddy stretches more in the y direction, since weak friction and thin boundary layers can only balance the vortex stretching associated with weak cross-isobath motion. These effects can also be seen in the distribution of kinetic energy. For two values of r, the vertically-averaged kinetic energy, KE = $\rho(U^2 + V^2)/2$, at given x, is calculated. It is shown in Fig. 3.4 that the energy distribution is more restricted

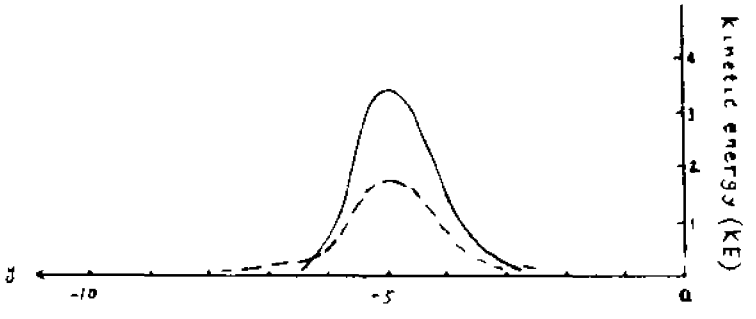

Figure 3.4: Distribution of kinetic energy as a function of y, at x = .8; corresponding to Fig. 3.2a (dashed line) and Fig. 3.2b(solid line).

by strong friction. These results are consistent with previous related studies (cf. Collings and Grimshaw, 1980; Louis and Smith, 1982). It is noted that the solution is not symmetric in the y-direction, due to the vorticity balance equation (2.11) being parabolic.

Consider motions in the northern hemisphere, i.e., $f > 0$. It can be seen from the form of the parameter C, that increasing (decreasing) f is the dynamical equivalent of decreasing (increasing) r. Physically, increasing rotation will decrease the Ekman layer thickness, so that the effect of the rotation on the circulation is inverse to that of the friction parameter. Thus, it is expected that if other conditions remain the same, then at lower latitudes the response of the shelf to oceanic forcing will be stronger than at higher latitudes. Similar arguments will be applicable if $f < 0$.

Next, the effects of varying the shelf steepness are examined. For a fixed shelf break depth, h_o, two values of the shelf width are selected: L_x = 100km, and L_x = 50km. The solutions for the sea surface displacement are shown in Fig. 3.5. Note that these are non-dimensional plots, where the dimensional x-unit is 100km in Fig. 3.5a, and 50km in Fig. 3.5b. A steeper shelf (narrower shelf width) leads to a stronger circulation. Again, this result may be understood by considering the vorticity balance. For shelves of the same depth, a narrower shelf means a greater topographic

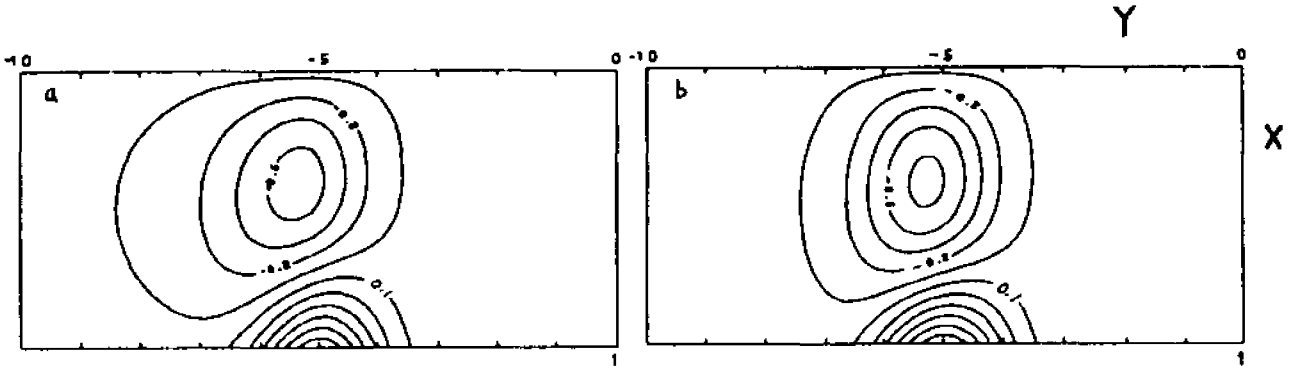

Figure 3.5: The dimensionless pressure field for a) L_x = 100km, and b) L_x = 50km.

gradient, ∇h. When forced fluid columns move a given distance across isobaths, intense relative vorticity will be generated over the narrower shelf because of greater vortex-tube stretching, i.e., greater $\nabla f \times \nabla h$ in the vorticity equation (3.4). To compensate this intense stretching, strong frictional vorticity generation is necessary, which is obtained by developing greater pressure gradients for given friction coefficients. Thus a stronger pressure field is maintained over the narrower shelf. By its influence on vortex-tube stretching, shelf geometry constrains the patterns of the circulation.

Finally, oceanic disturbances with varying alongshore scales are considered, corresponding to imposed pressure functions having different shapes, i.e., a pressure forcing function of small scale decays rapidly over a short dis-

tance, and a function of larger scale decays more slowly over a longer distance. The calculated solutions, for σ = 300km and 600km, are shown in Fig. 3.6, in which the dimensional y-unit is 600km. The imposed forcings result in altered patterns of shelf circulation. The shelf motion in

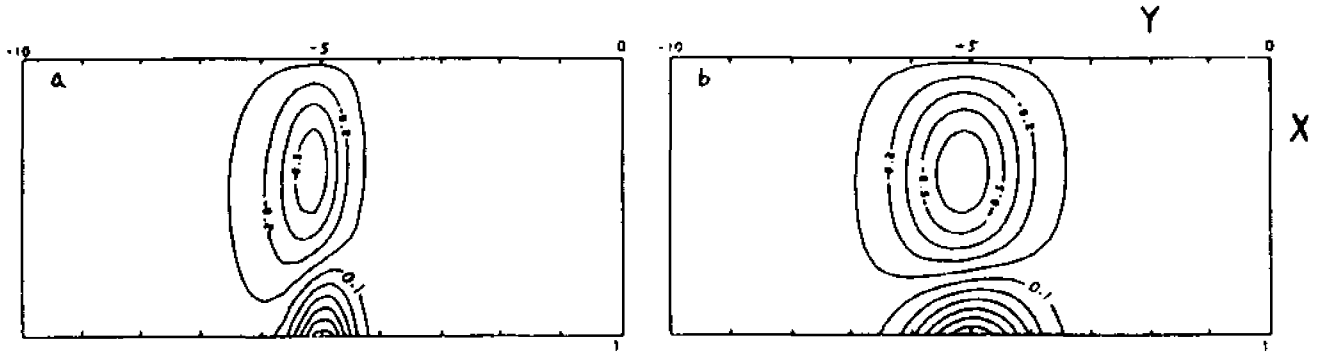

Figure 3.6: The pressure field for a) σ = 300km and b) σ = 600km.

response to narrow forcing is itself narrow and vice versa. In the case of narrow forcing, because the imposed pressure field drops rapidly away from the center of the forcing, the forced cross-isobath motion is strong and narrow, resulting in significant localized vortex-tube stretching which is balanced by frictional curl. Similarly, in the case of larger scale forcing, a weaker forced cross-isobath motion occurs over larger distances due to slow decay of the imposed pressure field. Vorticity production associated with this forced motion is broadly distributed, then it is dissipated by friction. This result demonstrates that the oceanic forcing impresses its scale on the shelf motion.

3.2 Curved shelf topography h=h(x,y)

In this subsection, the interaction of the oceanic disturbance with curved shelf topographies is considered. The longshore length scale, L_y, is assumed to be a shelf topographic scale, which may be greater, equal to, or smaller than that of the oceanic disturbance. A convergent shelf topography is assumed for which the transformation (2.15) is

$$\left.\begin{aligned} \xi &= x+(1-x)g(y) \\ \eta &= y \end{aligned}\right\}, \qquad (3.5)$$

where

$$g(y)=\{\tanh(y+y_0)-1\}/\{\tanh(y+y_0)+1\},$$

in which y_0 is a constant that can be selected for problems of interest (see Fig. 3.7 and Table 3.2).

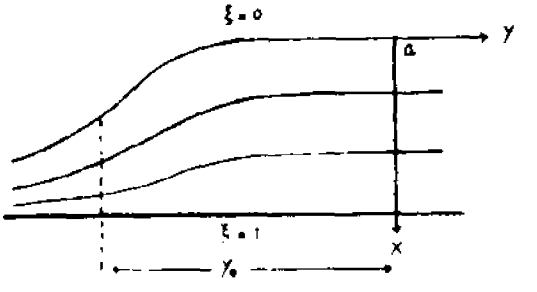

Figure 3.7: A sketch of the curved shelf topography.

The solution for ζ from (2.17) is, in terms of (ξ,η),

$$\zeta(\xi,\eta)=\sum_{n=1}^{\infty} X_n(\xi)Y_n(\eta)+\xi\exp(-(\eta+A)^2B), \qquad (3.6)$$

where

$$X_n(\xi) = \sin(n\pi\xi),\quad n = 1,2,3,\ldots$$

$$Y_n(\eta) = a_n e_+ + e_+\int_0^{\eta} e_- F_n^*(\eta')\, d\eta',$$

in which A is the central position of the disturbance at the offshore boundary, B is the ratio of longshore length scales, $(L_y/\sigma)^2$, and $F_n^*(\eta) = (-1)^{n-1}\, 4B(\eta+A)\exp(-(\eta+A)^2B)/n\pi$. a_n, e_+ and e_- are analytically calculated from (2.24). The velocities U and V are calculated from (2.7) and (2.8), remembering that

$$\frac{\partial \zeta}{\partial x} = \frac{\partial \zeta}{\partial \xi}\,\xi_x,$$

$$\frac{\partial \zeta}{\partial y} = \frac{\partial \zeta}{\partial \xi}\,\xi_y + \frac{\partial \zeta}{\partial \eta}\,\eta_y.$$

The solution (3.6) is similar to that for a straight shelf in that a vortex pair structure appears. However, alongshore topographic variation has influenced the solution (3.6) through the transformation (3.5). The importance of the topography to the resultant circulation patterns is again studied through numerical parametric analysis.

In the first set of experiments, only the location of the disturbance center is changed from A=3 to A=5 (Fig. 3.8). The solution shows clearly the topographically-induced asymmetry of the flow field. If the forcing is located far from the region of large topographic curvature, the resultant pressure field is similar to that over a straight shelf.

Table 3.2: Parameter values used in the dimensionless pressure field.

Varying Parameters	Constant Parameters	Nondimensional Parameters
a1 A = 3 a2 A = 5	$f = 10^{-4}\ s^{-1}$ $r = 1*10^{-4}\ ms^{-1}$ L_x = 100 km L_y = 600 km h_0 = 100 m σ = 600 km y_0 = 4	C = 15.0 B = 1.0 C = 15.0 B = 1.0
b1 $r = 1*10^{-4}\ ms^{-1}$ b2 $r = 5*10^{-4}\ ms^{-1}$	$f = 10^{-4}\ s^{-1}$ L_x = 100 km L_y = 600 km h_0 = 100 m σ = 600 km y_0 = 4 A = 5	C = 15.0 B = 1.0 C = 2.0 B = 1.0
c1 σ = 300 km c2 σ = 800 km	$f = 10^{-4}\ s^{-1}$ $r = 10^{-4}\ ms^{-1}$ L_x = 100 km L_y = 600 km h_0 = 100 m y_0 = 4 A = 5	C = 30.0 B = 4.0 C = 15.0 B = 0.5
d1 A = 4 d2 A = 3 d3 A = 2	$f = 10^{-4}\ s^{-1}$ $r = 1*10^{-4}\ ms^{-1}$ L_x = 100 km L_y = 600 km σ = 600 km h_0 = 100 m y_0 = 3	C = 15.0 B = 1.0 C = 15.0 B = 1.0 C = 15.0 B = 1.0

When the forcing is close to the location where h_y is large, the field is obviously intensified on the inshore side (Fig. 3.8b). The phenomenon may be understood by examining the vorticity dynamics. It is seen from the vorticity equation (3.4) that a longshore topographic variation generates a significant relative vorticity by vortex stretching when fluid columns move in the y-direction, which, then, requires a strong frictional dissipation in this region. This inten-

sified dissipation is obtained through an increased pressure gradient under the present parameterization of the stress law. Consequently, a strong pressure gradient develops

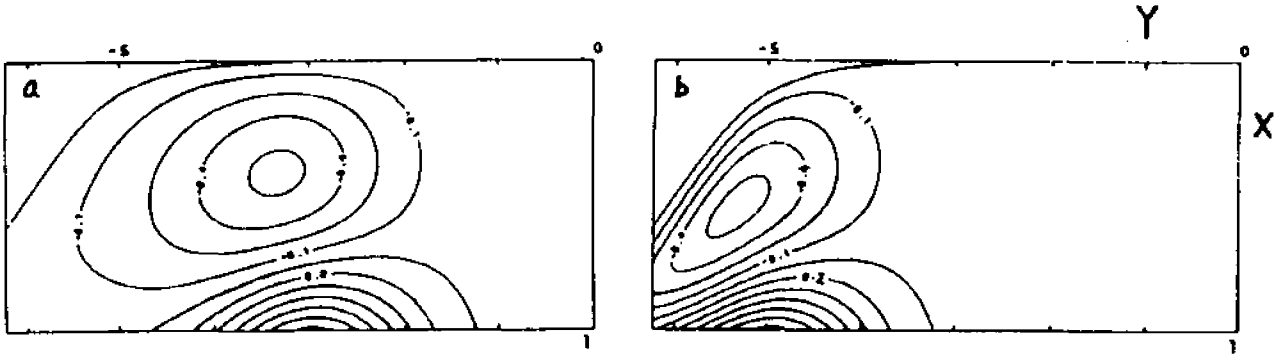

Figure 3.8: The dimensionless pressure field: a) A=3, and b) A=5

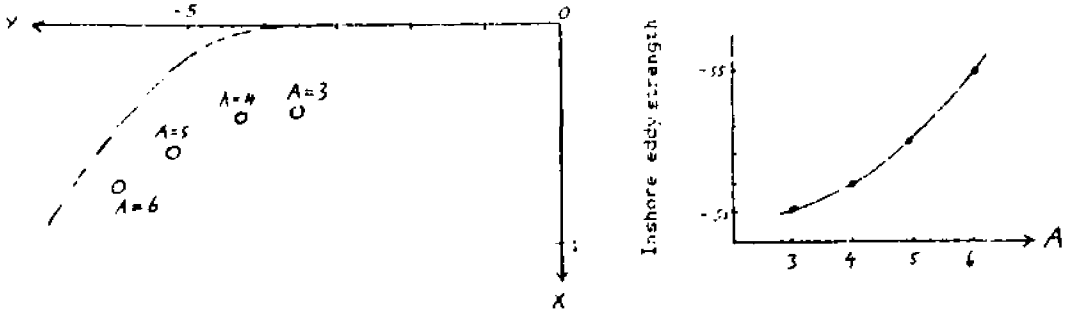

Figure 3.9: Center and strength of the inshore eddy as A varied. The dashed line is $\xi = 0$.

near the region of curvature, resulting in the asymmetry of the flow field. The center and strength of the inshore eddy, as A varies, are found numerically (Fig. 3.9). Comparing this with solutions for a straight shelf, it is seen

that when the curvature is present, because of the requirements of vorticity balance discussed above, as the center of the inshore eddy moves to the region where h_y is large, the strength of the inshore eddy increases. These results reveal the significant influence of the curved topography on the forced shelf motion.

Next, the combined effects of the friction and shelf curvature are investigated. The center of the disturbance is located at A = 5, and the resultant patterns for two values of r are compared. Now, for different values of r, the inshore boundary must lie along different depth contours consistent with the condition (2.9) and the transformation (3.5). A depth contour, ξ_1, is selected as an inshore boundary such that when $h_y \to 0$, then $\xi_1 \to x_1$, where x_1 is the inshore boundary for a straight shelf with the same r (Ref. subsection 3.1: Experiment a), $x = \{\xi_1 - g(y)\}/\{1-g(y)\}$ defines the boundary in the x-y system. Thus, for r=0.0001m/s, the inshore boundary occurs at $\xi_1 = 0.05$; for r=0.0005m/s, it occurs at $\xi_1 = 0.25$. The model solutions are shown in Fig. 3.10 and Fig. 3.11. The curved boundary lines are ξ=0, the coast. Again, an asymmetry of the pressure field occurs, induced by the lateral topographic variation. Moreover, it is interesting to find in Fig. 3.11a that increasing r leads to the center of the inshore eddy moving less far in the -y direction along the curvature. The presence of the curvature will cause vortex stretching when flu-

id columns move in the y-direction, and this action becomes more important if the motion is near the region of large

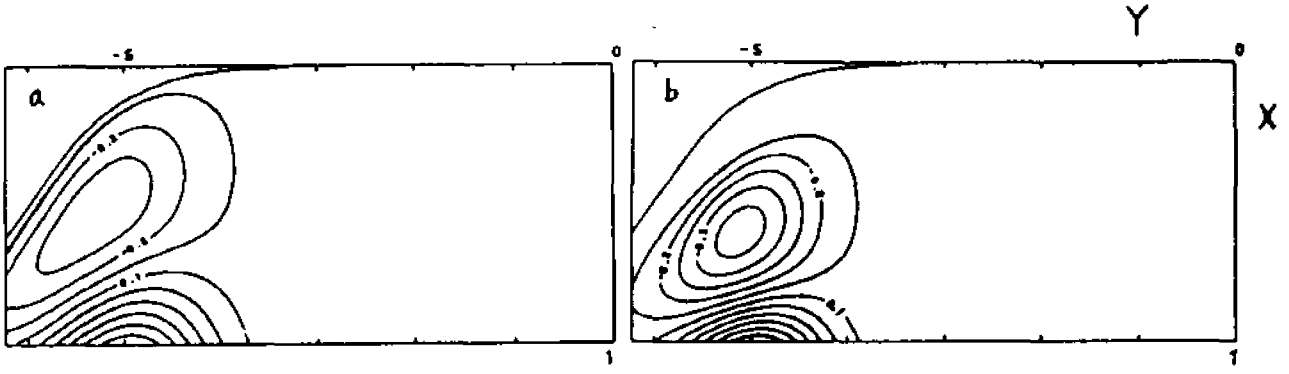

Figure 3.10: The dimensionless pressure field: a) r=0.0001m/s and b) r=0.0005m/s.

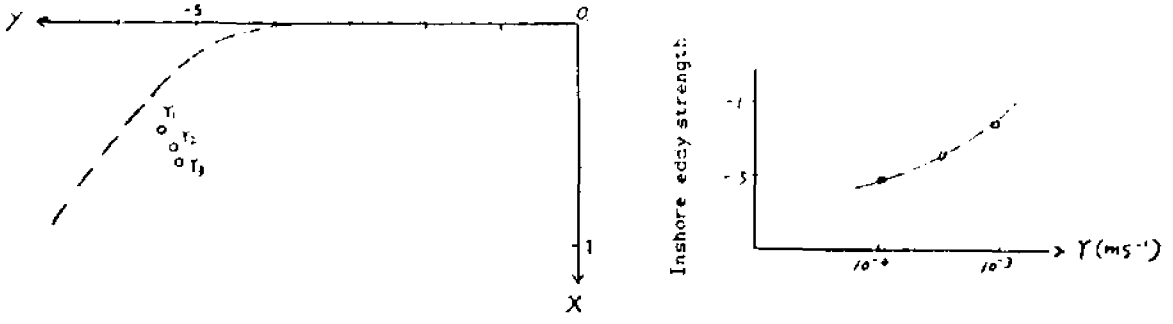

Figure 3.11: Center and strength of the inshore eddy as r varied. The dashed line is $\xi = 0$. r_i = 0.0001,0.0005,0.001m/s, i = 1,2,3.

curvature. On the other hand, strong friction (large r) will limit the motion spatially over the shelf. Thus, for strong friction, the impact of the curvature is less effective simply because the limited motion will restrict vortex

stretching near the region of large h_y . As discussed before, the movement of the center is not proportional to the migration of the inshore boundary as r is varied, therefore Fig. 3.11a shows a dynamical influence of the friction on the position of the inshore eddy in the presence of curvature. The combined effect of curvature and strong friction give rise to a greater strength of the inshore eddy, as shown in Fig. 3.11b.

In the third experiment, the combined effect of forcing scale and shelf curvature is examined. Forcings with various scales have different shapes, as described in subsection 3.1, Experiment c. In Fig. 3.12, the presence of large curvature only induces a weak asymmetric inshore eddy for small scale forcing, but an intense asymmetric eddy for large scale forcing. The large curvature acts as a source of vorticity when fluid columns move in the y-direction. This action is more effective when large scale forcing

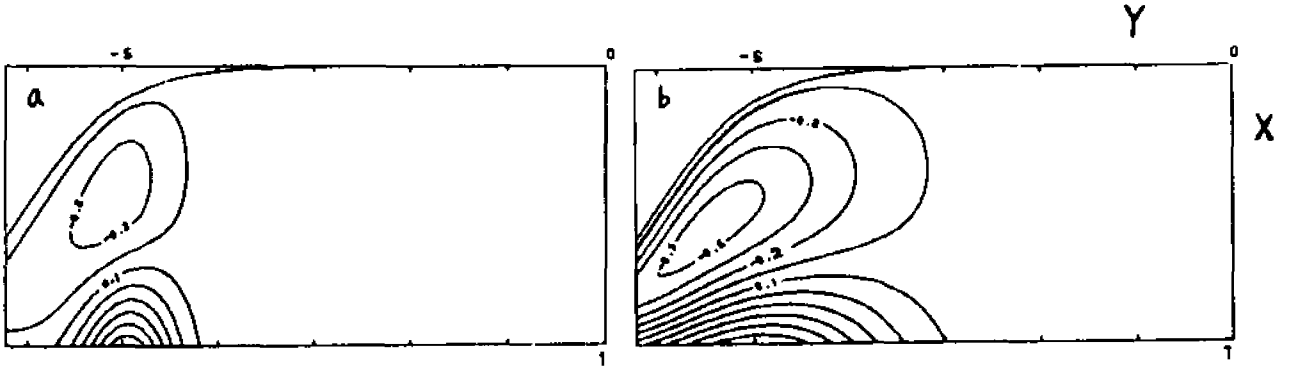

Figure 3.12: The dimensionless pressure field: a) σ = 300km, and b) σ = 800km.

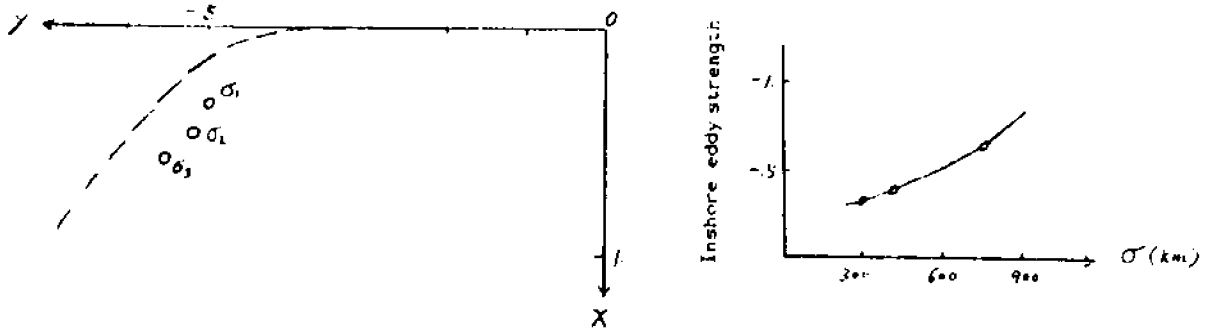

Figure 3.13: Center and strength of the inshore eddy as σ varied. The dashed line is ξ = 0. σ_i=300, 420, 800 km, i = 1,2,3.

drives strong motion in the y-direction. Vortex stretching generates significant relative vorticity that is dissipated by strong friction, resulting in the intense flow field observed over the inshore region. Conversely, the curvature is less effective for small scale forcing due to weak forced motion in the y-direction. Consequently, the flow field is only slightly compressed inshore by the curvature. As the scale of the oceanic forcing increases, the center of the inshore eddy will move along the curvature and increase in strength, as shown in Fig. 3.13.

Finally, a symmetric curved topography is considered such that

$$\left.\begin{aligned} \xi &= x+(1-x)g(y) \\ \eta &= y \end{aligned}\right\}, \qquad (3.7)$$

where

$$g(y) = 1 - \cosh(y+y_0).$$

A sketch of the topography, which represents a coastal embayment or trough, is given in Fig. 3.14. Solutions, with

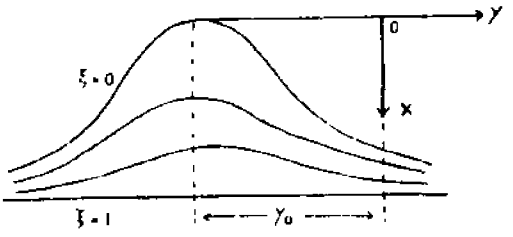

Figure 3.14: A sketch of the symmetric topography.

the center of the disturbance located at A = 2, 3, and 4, are shown in Fig. 3.15. Other parameters of the problem are listed in Table 3.2. An interesting feature is that although the forcing centers, A = 2 and A = 4, are symmetric about the center of the curved topography (y=-3), the two solutions are not 'symmetric'(see Fig. 3.15a and 3.15c).

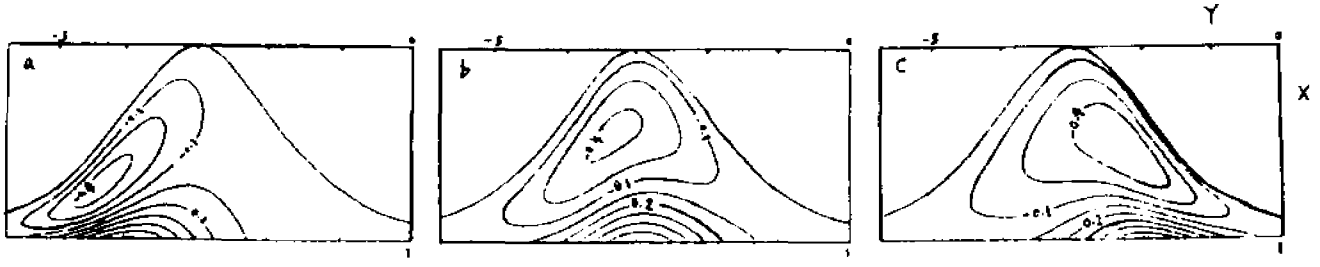

Figure 3.15: The dimensionless pressure field: a) A = 4, b) A = 3, and c) A = 2.

This results from asymmetric vorticity input due to the curved topography. From the transformation (3.7), $h_y = -\sinh(y+y_o)(1-x)$, thus h_y is decreasing when $y > y=-3$, and increasing when $y < y=-3$. Hence, if the forcing is imposed at A=2 ($y > y=-3$), vortex-tube stretching is negative when fluid columns move in the + y-direction because of the decreased topographic gradient, but this stretching is positive if the forcing is imposed at A=4 ($y < y=-3$) due to increased h_y. The pressure fields associated with the dissipation of vorticity appear asymmetric.

Chapter IV

DISCUSSION

It has been shown in the above analysis that, given a steady isolated barotropic oceanic disturbance as forcing at the shelf break, an approximately dipolar structure of the flow field occurs as the response over the shelf. An explanation of this is given in the appendix, and the essence of the theory lies in the assumption of an isolated system. This solution may be considered as damped topographic Rossby waves generated by an eddy or a meander impinging on the continental margin. To see this possible relation, start with the linearized, viscid, vertically-integrated equations of motion in the absence of wind stress:

$$U_t - fV = -g\,\zeta_x - rU/h, \qquad (4.1)$$

$$V_t + fU = -g\,\zeta_y - rV/h, \qquad (4.2)$$

$$(hU)_x + (hV)_y = -\zeta_t. \qquad (4.3)$$

If harmonic time dependence is assumed, i.e., $\zeta(x,y,t) = \mathrm{Re}\{\overline{\zeta}(x,y)\exp(-i\omega t)\}$, $U(x,y,t) = \mathrm{Re}\{\overline{U}(x,y)\exp(-i\omega t)\}$, $V(x,y,t) = \mathrm{Re}\{\overline{V}(x,y)\exp(-i\omega t)\}$, then it may be shown that $\overline{U}$ and $\overline{V}$ are given by

$$\overline{U} = g\{-\overline{\zeta}_y + i\kappa\overline{\zeta}_x\}/f(1-\kappa^2),$$

$$\overline{V} = g\{\overline{\zeta}_x + i\kappa\overline{\zeta}_y\}/f(1-\kappa^2),$$

where $k = \omega/f + ir/fh$. For $(\omega/f)^2 \ll 1$, $(r/fh)^2 \ll 1$, substituting $\bar{U}$, $\bar{V}$ into (4.3) produces, after neglecting the surface divergence,

$$\nabla\bar{\zeta}\times\nabla h + \{[(i\omega h-r)\bar{\zeta}_x]_x + [(i\omega h-r)\bar{\zeta}_y]_y\}/f = 0. \quad (4.4)$$

From (4.4) the quasi-steady limit

$$\nabla\bar{\zeta}\times\nabla h - \{\bar{\zeta}_{xx} + \bar{\zeta}_{yy}\}r/f = 0 \quad (4.5)$$

is obtained if $r/h \gg \omega$. Equation (4.5) is identical to the vorticity equation (2.6) derived in chapter 2. Thus it is shown here that, at very low frequency and for sufficiently strong friction, there may be forced damped topographic Rossby waves over the shelf, whose quasi-steady state might produce a mean pressure field. In the case of isolated oceanic forcing, the damped topographic Rossby waves appear as an eddy-like mean pressure field over the shelf. It should be pointed out that, because the waves do not arise through vorticity change due to coastal Ekman divergence by the wind, a coastal boundary appears not to be important in their generation, and the waves are not trapped nearshore. Furthermore, the oceanic disturbance is isolated. Thus, it can only force localized motion by direct vorticity injection onto the shelf or advection across a vorticity gradient, and the presence of an 'undisturbed' inshore boundary maintains this quasi-steady, isolated system. In fact, a connection between the presence of the topographic Rossby waves on the shelf and oceanic eddies/meanders approaching

the continental margin has been suggested from observations, e.g., Garrett (1979); Louis and Smith (1982). Thus this paper seems, for the first time, to show theoretically that this connection may well exist even in a quasi-steady state, i.e., that as the Rossby waves propagate onto the shelf, a mean flow field may be sustained in the presence of strong friction. Hence the proposed concept is based on the dynamical equations discussed above and the observations presented in the literature to date. This is the most interesting result of the present study.

This study has shown that friction significantly changes the structure of the circulation, a result which is not clearly seen in previous studies. Perhaps, because of the assumptions of isolated forcing and no surface stress, the dynamic role of friction in the circulation can be more directly resolved. The process through which the frictional stress curl balances the vortex stretching is clarified in (3.4),

$$(\nabla\zeta\times\nabla h)g/f - w_{\bullet} = 0. \qquad (4.6)$$

In terms of the proposed concept of topographic Rossby waves, (4.6) implies that the energy carried by the waves is dissipated in the bottom boundary layer. This layer supports Ekman pumping, so that a quasi-steady state involving mean pressure gradients at angles to the topographic gradients can be reached. Further, it is noted from (4.6) that

the Ekman vertical velocity may be positive or negative, dependent on the direction of flow and, therefore, vortex stretching. Thus, the presence of a sloping bottom breaks down the usual assumption of isotropy of the Ekman pumping within an eddy. This implies that, if a vortex is maintained over the shelf, there may be upwelling on one side of the eddy, but downwelling on another.

This work can be compared with other theoretical studies. The localized dipolar flow field here is not seen in Csanady's solution (1978), because he imposes a constant pressure gradient with infinite scale at the shelf break, i.e. the forcing is not localized. Kelly and Chapman (1988) numerically investigate steady deep-ocean eddy forcing in a stratified fluid. They find that a single eddy causes a jet trapped over the upper slope with the alongshore velocity in the jet directed opposite to that in the eddy. The dynamic difference between their work and this study is the stratification included in their work. This allows vertical shear of the flow field that may still satisfy the requirement of zero net relative angular momentum without causing countercurrents inshore. Also, the forcing is imposed at the shelf break in the present work, while in their model the forcing is imposed over the deep ocean. There is a modest volume of literature discussing the insulating role of the continental slope in such cases, e.g., Wang, 1982; Csanady and Shaw, 1983. Regarding the effect of curved topography on steady

shelf motion, this study shows that when alongshore topographic variation is large, a lateral coastal boundary has an important effect on the shelf response. This effect is stronger than that for small-amplitude coastline perturbations studied previously (e.g., Killworth, 1978).

The present solution has features similar to those of some laboratory experiments. By producing an isolated barotropic disturbance on a β-plane in a sliced-cylinder, Firing and Beardsley (1976) observed that the flow field relaxed to a dipolar structure. In their experiments, the β-effect was modeled by a change in depth h, dynamically equivalent to the forced shelf motion on the f-plane with a sloping bottom. In a homogeneous fluid, Flierl et al. (1983) imposed a point source in a rotating tank, and, after two periods of rotation, they observed the formation a vortex pair which persisted for a much longer time. Although not directly comparable with these time-dependant experimental studies, this study seems to describe aspects of the quasi-steady state realized in the laboratory.

No observational data sets have been found which are appropriate for direct comparison with the present model. There are data available, though, which do not satisfy all the scaling requirements of the model, but do exhibit certain features of the model solution. It is, thus, instructive to compare the model predictions with the observations for such a situation. One example is circulation on the

Louisiana-Mississippi-Alabama shelf (LMAS). Fig. 4.1 shows the annual mean geopotential topography on LMAS (Dinnel, 1988). Choosing appropriate values, an analytic curve-fit to the real LMAS topography is illustrated in Fig. 4.2, where the 20m isobath is selected as an inshore boundary of the model. A Gaussian forcing function is compared with measurements in Fig. 4.3. The measurements represent the dynamic height at the sea surface along the 100m isobath, with respect to 500db. These were calculated by integrating along the bottom (Dinnel, 1988), and then subtracting 74 dynamic centimeters, a process which does not alter the dynamically important gradients. While the dynamic topography represents a baroclinic signal, the similarity of the 0 and 50 db dynamic height suggests that there is a barotropic pressure gradient imposed at the shelf break. It may be overestimated by using the 0/500 db topography, though. Based on these measurements, parameters A and B of the Gaussian function are determined as follows: 1) the position of the highest surface geopotential is chosen as the center of the forcing, here A = 1.5, 150km from the coordinate origin (see Fig. 4.2); 2) B = $L_y^2/(2\sigma^2)$, where L_y = 100km, calculated from the boundary function (3.5), and σ = 35km from a least-squares fit to the observations, thus B = 4.1.

Using the fitted Gaussian function and the curved topography, the solution is shown in Fig. 4.4. It is assumed that the 0/500 db dynamic height gradients equal the sea surface

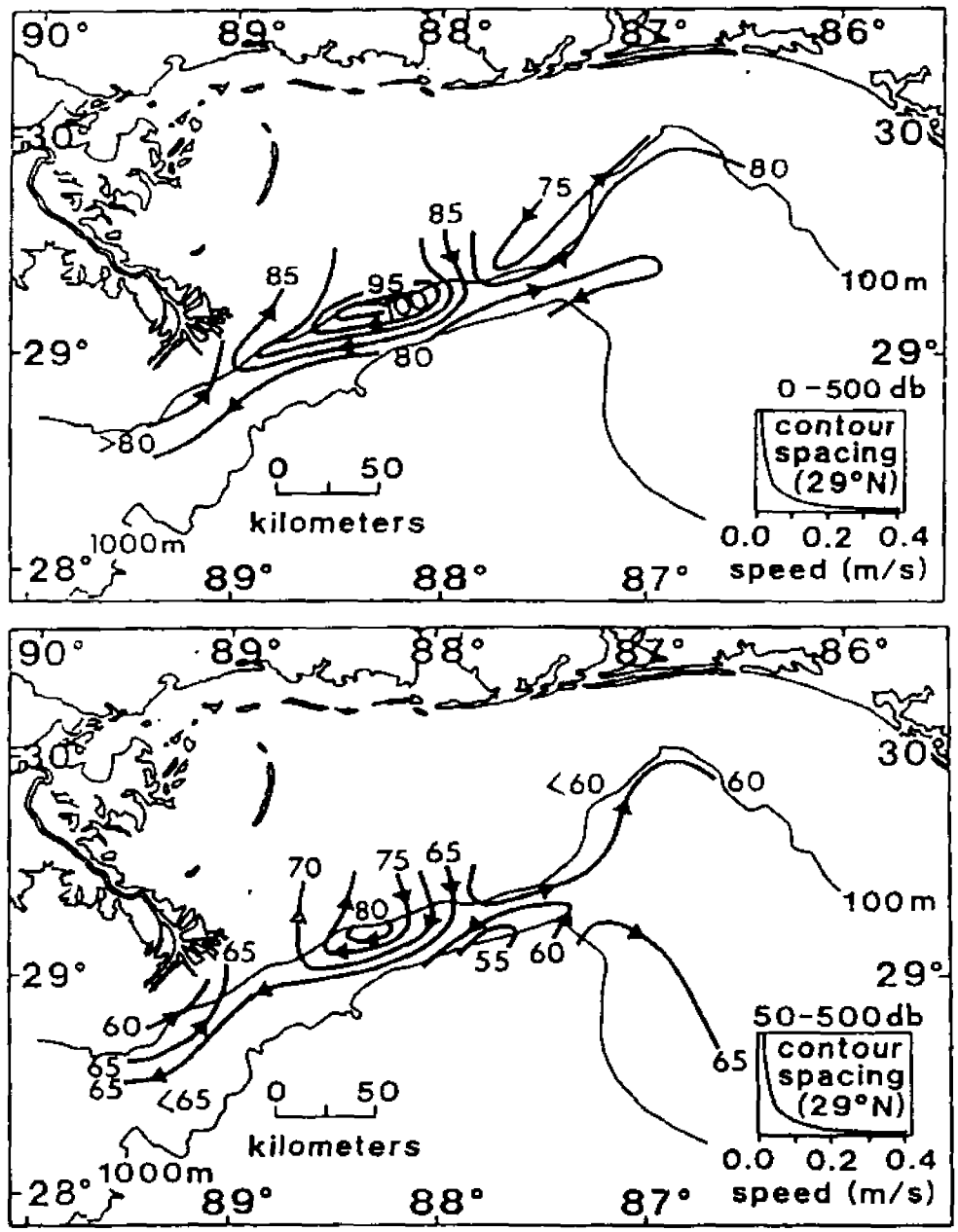

Figure 4.1: Annual mean surface geopotential topography, a) 0/500 db and b) 50/500 db. Contours are in dynamic centimeters.

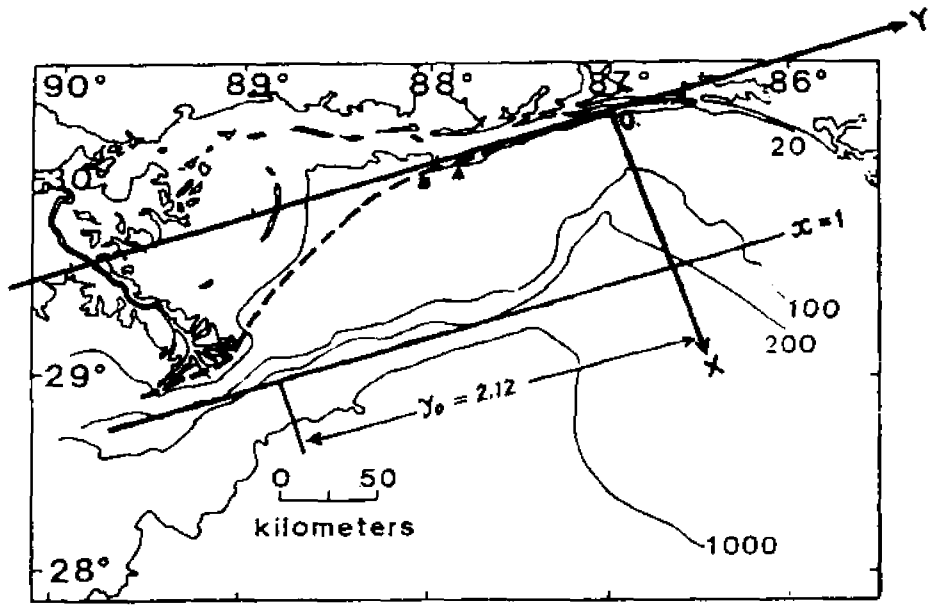

Figure 4.2: Domain of the model and LMAS. A dashed line is the model boundary. Isobaths are in meters. A square and a triangle are locations of current meter moorings from Chuang et al, 1982 and Dinnel, 1988.

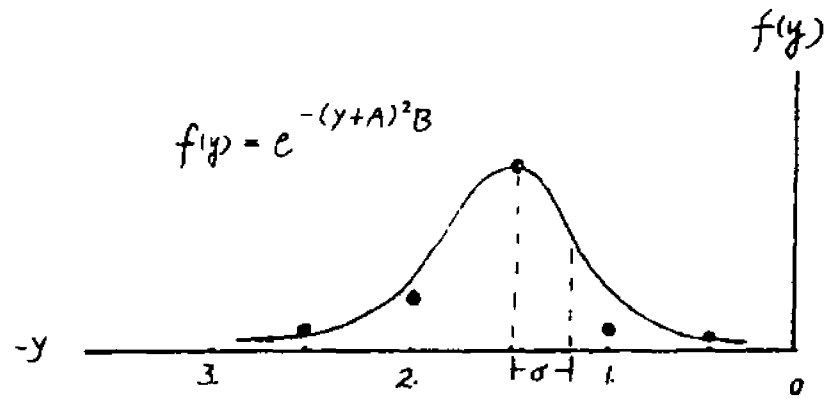

Figure 4.3: Comparison of the forcing function used in the model and the measurements. '●' are the measurements.

height gradients, thus in Fig.4.4 the sea surface is pre-

sented in dimensional units of centimeters. In Fig 4.5, at y = -150km (the dashed line in Fig. 4.4), the y-direction geostrophic velocity is calculated as a function of x. The dipolar pattern, i.e., an eastward flow over

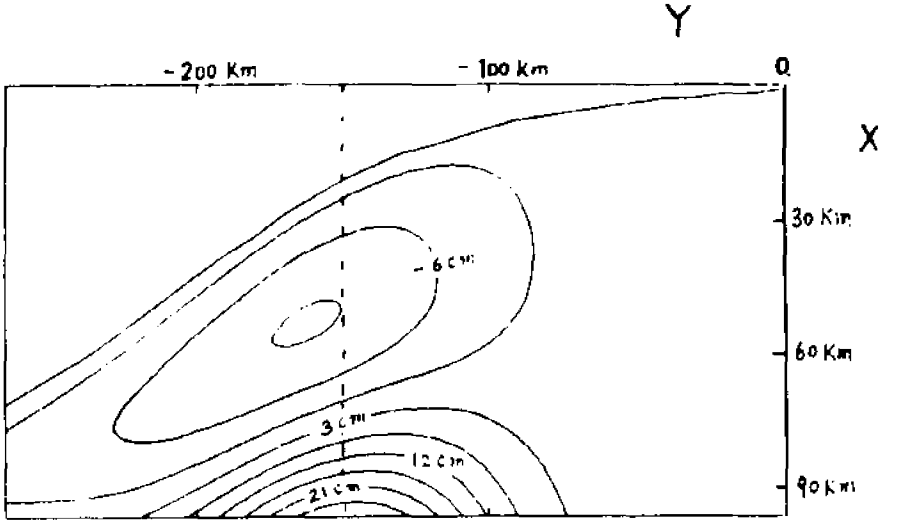

Figure 4.4: The dimensional sea surface in centimeters. r = 0.0003m/s. The dashed line is at y = -150km, at which the y-dirction velocity v is calculated (Fig. 4.5).

the outer LMAS and a cyclonic circulation on the inner shelf, is consistent with that inferred by previous authors (eg., Schroeder et al, 1987; Dinnel, 1988). Over seasonal time scales, these authors observed westward flow inshore and eastward flow over the outer shelf, which could not be totally explained by the wind forcing. They proposed that extensions of the Loop Current might drive LMAS currents. To quantitatively compare the solution with the field data, from Fig. 4.5, a nearshore geostrophic speed (30°N, 88°S) of

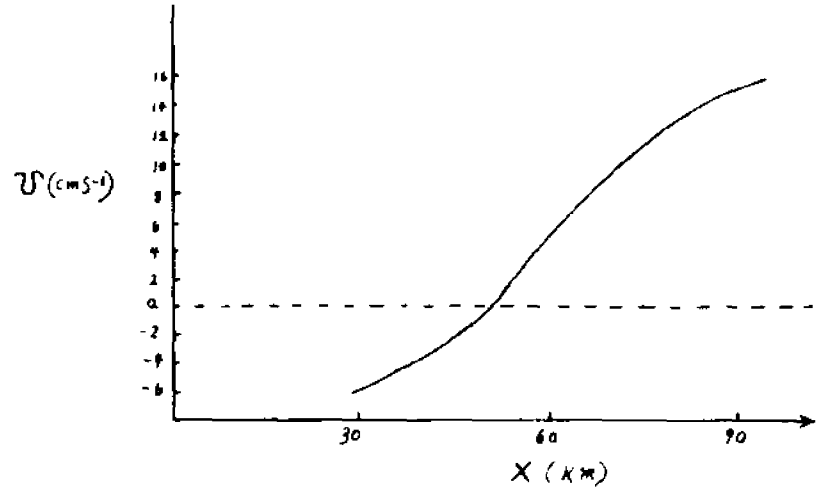

Figure 4.5: The y-direction geostrophic velocity, v, as function of x, at y = -150km. Positive v points to the east.

about 5 cm/s is estimated. If the frictional dissipation, calculated as ζ_y rg/(f^2h) {equation (2.8)}, is included, then a mean westward flow of approximately 4 cm/s is found. This is in agreement with previous long-term observations in the same region (Chuang et al, 1982; Dinnel 1988; see Fig. 4.2 for the mooring locations). While this model does predict some of the observed features of circulation on LMAS, it should be noted that, in this case, $(L_x/L_{y,t})^2$ = 0.25, and $L_x/L_{y,o})^2$ = 1. Thus the condition (2.10) is not satisfied. This might cause alongshore flow to be overestimated (Kelly and Chapman, 1988). Furthermore, there were slight vertical shears in the data (Fig. 4.1), so this barotropic solution is, at best, only approximately valid. In spite of

these limitations, evidence from the observations (e.g., Dinnel, 1988) suggests the plausibility of isolated ocean-driven circulation on LMAS similar to this study. The westward mean current was not related to the prevailing wind direction. The efficiency of the time-varying wind in setting up the currents was asymmetric, suggesting that ocean-driven currents might flow against the wind-driven currents. The westward mean currents increased with distance from shore, while wind-driven coastal currents normally decrease with distance from the coast. It seems that the ocean-driven motion, at least, partially contributes to the circulation on LMAS.

The present study may have implications for shelf management. The solution shows that, given an isolated oceanic forcing at the shelf break, an eddy-like flow field forms inshore. If, however, pollutants were accidentally released into the center of the eddy, severe environmental contamination would be expected around the region, as the pollutants would be trapped within the recirculation zone. Such eddy-currents may affect biological processes as well. For example, upwelling or downwelling within the eddy may cause primary production to vary significantly by effecting the vertical flux of nutrients. Ultimately, this will cause changes in secondary production. If the eddy occurs in the spawning region of a shelf spawner, such as menhaden or shrimp, then the eggs and larvae may be trapped. Thus cir-

culation within the eddy may enhance or reduce fish recruitment.

Extensive further investigation is needed to understand ocean-driven shelf motion. It is necessary to explore the initial value problems of the shelf motion, i.e., the spin-up of such forced motions, which was not considered at the present work. Nonlinear and stratification effects should also be considered in further studies.

Chapter V

CONCLUSIONS

For a barotropic case, steady shelf motion forced by an isolated oceanic disturbance has been analytically studied, using a linear, viscid, vertically-integrated model. Only bottom frictional stress is considered here, which is parameterized by the linear stress law with a constant friction coefficient. Surface stress is assumed to be zero in this work. From this study, the following conclusions can be stated:

(1) The solution generally shows a dipolar structure of the flow field over the shelf, which has not been discussed in previous studies. Considering the isolated oceanic forcing and the 'undisturbed' inshore boundary, this solution is a simple representation of an isolated system with zero net relative angular momentum (see appendix).

(2) The parametric studies show that the forced circulation patterns appear to be controlled by the length scale of the forcing, magnitude of bottom friction, and geometry of the shelf. The scale of the shelf response is, generally, similar to the scale of the forcing, though, the response may extend downcoast for small r. The strength of the fric-

tion parameter alters the structure of the response. Stronger friction maintains greater pressure gradients within a narrower area, and causes the center of the inshore eddy to move seaward with greater strength. The shelf geometry influences the strength of the response through the vortex- stretching effect. When large longshore topographic gradients are present, the previously described response is amplified for a convergent topography and vice versa for a divergent topography.

Appendix A

AN INTEGRAL THEOREM

An integral theorem of zero net relative angular momentum is proved, extending the integral theorems of Flierl et al.(1983) to an isolated system on the f-plane with a sloping bottom. The basic concepts are the isolation and quasi-steady state of the oceanic disturbance, introduced in chapter 1. Other assumptions are the same as discussed in chapter 2. For simplicity, it is assumed here that a linear sloping bottom varies in the x-direction only, although some more complicated cases may be possible for the proof.

Consider the cross-shelf (x) momentum equation and the mass conservation equation

$$\frac{\partial u}{\partial t} + \nabla\cdot(Vu) - fv = -g\frac{\partial p}{\rho\partial x} + \frac{\partial T_{zx}}{\rho\partial z},$$

$$\nabla\cdot(\rho V) = 0,$$

where $V = ui + vj + wk$. The integrated form of the mass conservation equation gives nondivergence of the horizontal mass transport, hence a streamfunction $\Psi(x,y,t)$ can be defined by

$$\int \rho u dz = -\Psi_y, \qquad \int \rho v dz = \Psi_x.$$

The three-dimensional integrals of the momentum equation are

$$\frac{\partial}{\partial t}\iint dxdyh\int udz + \iint dxdyh\int \nabla\cdot(Vu)dz - f\iint dxdyh\int vdz$$

$$= -g/\rho\iint dxdyh\int P_x\, dz - r\iint dxdy\int udz, \qquad (A1)$$

the integrals being taken over the region $x \in (0, L_x)$, $y \in (-\infty, +\infty)$, and $z \in (-h, \eta)$; the surface stress being taken to be zero in (A1), as before. The integral of the time derivative term vanishes because of the restriction of slowly varying motion, as does the integral of nonlinear terms, due to sufficiently rapid decay of the velocity field far from the disturbance. The first term on the right-hand side of (A1) can be written as

$$-g/\rho\iint dydz\int\{(Ph)_x - h_xP\}dx,$$

which vanishes, as the pressure field $p \to 0$ with increasing y for the spatially isolated system. Finally, the second term on the right-hand side of (A1) vanishes, provided $u \to 0$ quite rapidly from the center of the disturbance. Thus it is concluded that

$$-f\iint dxdyh\int vdz = 0,$$

which is equivalent to

$$f\iint \Psi dxdy = 0. \qquad (A2)$$

Note that the net relative angular momentum is

$$L_z = \iint \rho R\times V d\tau = \rho\iint dxdy\int dz(xv-yu) = 2\iint \Psi dxdy,$$

then, from (A2), it is obtained that

$$L_z = 0, \qquad \text{(A3)}$$

to a good approximation.

It is obvious in deriving the theorem that, were the surface stress not zero, the theorem could not be proved because the system would no longer be 'isolated' if there were wind stress forcing all over the area. Neither can the theorem be proved in the case of non-isolated oceanic forcing. In this sense, the theorem demonstrates why the solution of this study looks quite different from that of Csanady's work(1978). It is noted likewise that when the β-effect is absent, the sloping topography plays a key role in the proof of the theorem, implying the important physical fact that the penetration of the disturbance onto the continental shelf may be severely limited by topographic constraints and by bottom viscous dissipation, which are shown clearly in the solutions of chapter 3. On the whole, this theorem shows that even for homogeneous fluid on an f-plane, if the forcing is self-contained and the system remains 'isolated' by the topographic constraints and the frictional dissipation, then dipolar structures of the motion will be a necessary consequence of such a system.

REFERENCES

1. Allen, J. S., 1976: Continental shelf waves and alongshore variations in bottom topography and coastline. J. Phys. Oceanogr., 6, 864-878.
2. Brooks, D. A., and J. M. Bane, Jr., 1983: Gulf Stream meanders off North Carolina during winter and summer, 1979. J. Geophys. Res., 88, 4633-4650.
3. Chuang, W. S., W. W. Schroeder, and W. J. Wiseman, Jr., 1982: Summer current observations off the Alabama coast. Contributions in Marine Science, 25, 121-131.
4. Churchill, J. H., P. C. Cornillon and G. W. Milkowski, 1986: A cyclonic eddy and shelf-slope water exchange associated with a Gulf Stream warm-core ring. J. Geophys. Res., 91, 9615-9623.
5. Collings, I. L., and R. Grimshaw, 1980: The effect of current shear on topographic Rossby waves. J. Phys. Oceanogr., 10, 363-371.
6. Csanady, G. T., 1978: The arrested topographic wave. J. Phys. Oceanogr., 8, 47-62.
7. _____, G. T., and P. T. Shaw, 1983: The "insulating" effect of a steep continental slope. J. Geophys. Res.,88, 7519-7524.

8. Dinnel, S. P., 1988: Circulation and sediment dispersal on the Louisiana-Mississippi-Alabama continental shelf. Ph.D. Dissertation, LSU.

9. Firing, E., and R. C. Beardsley, 1976: The behavior of a barotropic eddy on the deta plane. J. Phys. Oceanogr., 6, 57-65.

10. Flierl, G. R., M. E. Stern, and J. A. Whitehead, 1983: The physical significance of modons: Laboratory experiments and general integral constraints. Dyn. Atmos. Oceans, 7, 233-263.

11. Garrett C., 1979: Topographic Rossby waves off East Australia: identification and role in shelf circulation. J. Phys. Oceanogr., 9, 244-253.

12. Garvine R. W., K.-C. Wong, G. G. Gawarkiewicz, and R. K. McCarthy, 1988: The morphology of shelfbreak eddies. J. Geophys. Res., 93, 15593-15607.

13. Huh, O. K., W. J. Wiseman, Jr., and L. J. Rouse, Jr., 1981: Intrusion of Loop Current waters onto the West Florida Continental Shelf. J. Geophys. Res., 86, 4186-4192.

14. Huyer, A., R. L. Smith, P. J. Stabeno, J. A. Church and N. J. White , 1988: Currents off south-eastern Australia: results from the Australian Coastal Experiment. Aust. J. Mar. Freshwater Res., 39, 245-288.

15. Kelly, K. A., and D. C. Chapman, 1988: The response of stratified shelf and slope waters to steady offshore forcing. J. Phys. Oceanogr., 18, 906-925.

16. Kennett, J. P., 1982: Marine Geology. Prentice-Hall, Inc. 813pp.

17. Killworth, P. D., 1978: Coastal upwelling and Kelvin waves with small longshore topography. J. Phys. Oceanogr., 8, 188-205.

18. Kroll, J., and P. P. Niiler, 1976: The transmission and decay of barotropic topographic Rossby waves incident on a continental shelf. J. Phys. Oceanogr., 6, 432-450.

19. Louis, J. P., and P. C. Smith, 1982: The development of the barotropic radiation field of an eddy over a slope. J. Phys. Oceanogr., 12, 56-72.

20. Middleton, J. H., 1987: Steady coastal circulation due to oceanic alongshore pressure gradients. J. Phys. Oceanogr., 17, 604-612.

21. Mitchum, G. T., and A. J. Clarke, 1986: The frictional nearshore response to forcing by synoptic scale winds. J. Phys. Oceanogr., 16, 934-946.

22. Morse, P. M., and H. Feshbach, 1953: Methods of theoretical physics. Int. Ser. in Pure and Applied Physics, Mcgraw-Hill Book Company, 1978pp.

23. Schroeder, W. W., S. P. Dinnel, W. J. Wiseman, Jr., and W. J. Merrell, Jr., 1987: Circulation patterns inferred from the movement of detached buoys in the eastern Gulf of Mexico. Continental Shelf Res., 7, 883-894.

24. Smith, IV, D. C., 1986: A numerical study of Loop Current eddy interaction with topography in the western Gulf of Mexico. J. Phys. Oceanogr., 16, 1260-1272.

25. Wang, D. P., 1982: Effects of a continental slope on the mean shelf circulation. J. Phys. Oceanogr., 12, 1524-1526.

VITA

Xinyu He was born on 29 April 1956 in Beijing, China. She received her B.S. in Physics from Jilin University, China and M.S. in Physical Oceanography from Ocean University of Qingdao, China. On completion of her Ph.D, she will take the position of Post-doc/Research Associate in Geophysical Fluid dynamics, School of Mathematics, University of New South Wales, Australia.

DOCTORAL EXAMINATION AND DISSERTATION REPORT

Candidate: Xinyu He

Major Field: Marine Sciences

Title of Dissertation: Barotropic Shelf Circulation Forced by an Isolated Oceanic Disturbance

Approved:

Major Professor and Chairman

Dean of the Graduate School

EXAMINING COMMITTEE:

Stephen P. Murray

George D. Cataland

Stephen A Harrison

J R Dorroh

Date of Examination:

April 28, 1989